J. Meas. Sci. Instrum., 2025, 16(2): 272-279. http://jmsi.publish.founderss.cn
DOI: 10.62756/jmsi.1674-8042.2025026 jmsi@nuc.edu.cn

Sensing characteristics of feedback waveguide slot grating microring resonators

ZHU Yanjie, LIANG Longxue*, LIU Chunjuan

School of Electronic and Information Engineering, Lanzhou Jiaotong University, Lanzhou 730070, China

***Corresponding author:** LIANG Longxue (llxue@mail.lzjtu.cn)

Received: September 3, 2024 **Revised:** October 15, 2024 **Accepted:** October 29, 2024

Abstract: To enhance the quality factor and sensitivity of refractive index sensors, a feedback waveguide slot grating micro-ring resonator was proposed. An air-hole grating structure was introduced based on the slot micro-ring, utilizing the reflection of the grating to achieve the electromagnetic-like induced transparency effect at different wavelengths. The high slope characteristics of the EIT-like effect enabled a higher quality factor and sensitivity. The transmission principle of the structure was analyzed using the transmission matrix method, and the transmission spectrum and mode field distribution were simulated using the finite-difference time-domain (FDTD) method, and the device structure parameters were adjusted for optimization. Simulation results show that the proposed structure achieves an EIT-like effect with a quality factor of 59 267.5. In the analysis of refractive index sensing characteristics, the structure exhibits a sensitivity of 408.57 nm/RIU and a detection limit of 6.23×10^{-5} RIU. Therefore, the proposed structure achieved both a high quality factor and refractive index sensitivity, demonstrating excellent sensing performance for applications in environmental monitoring, biomedical fields, and other areas with broad market potential.

Key words: integrated optics; micro-ring resonator; slot micro-ring; grating; refractive index sensor; silicon waveguide

0 Introduction

With the rapid development of silicon-on-insulator (SOI) technology, optical devices based on the SOI platform attract widespread attention due to their fast response speed, strong electromagnetic interference resistance, and ease of integration[1]. Researchers propose many optical sensors based on the SOI platform, such as one-dimensional photonic crystal sensors[2,3], micro-ring/micro-disk resonators[4], surface plasmon sensors[5], and sub-wavelength grating sensors[6]. Among various optical sensors, the micro ring resonator (MRR) garners significant attention due to its low insertion loss, high quality (Q) factor, and compact structure[7]. It is widely used in fields such as medical diagnosis[8], environmental monitoring, and national security. However, the sensing performance of traditional MRRs is often limited by the symmetric Lorentzian line shape[9], resulting in lower quality factors and sensitivities, which is challenging to meet the demands of sensing applications.

To enhance the sensing performance of micro-ring resonators, researchers have developed various innovative structures. For instance, adding a U-shaped feedback waveguide segment to a double-channel micro-ring resonator (MRR) can introduce additional light fields, resulting in Fano-type transmission spectra[10]. Another approach involves combining double-channel racetrack MRRs with gratings to achieve high-slope Fano resonance[11]. Inserting air holes in the straight waveguide at the coupling position of the MRR was used to control the transmission spectrum shape[12]. Additionally, integrating MRRs with photonic crystal structures can produce EIT-like effects (electromagnetically induced transparency)[13]. The groove micro-ring and slot phase-shifting Bragg grating bus straight waveguide coupling structure[14] demonstrated a device sensitivity of 297.13 nm/RIU, but the quality factor was only 2 000, with a sensitivity detection limit of 1.1×10^{-4} RIU. Another reported structure[15] had a quality factor as high as 1.9×10^{5}, but the sensitivity was only 86.371 4 nm/RIU. The compact inner-wall grating micro-ring resonator boasted a refractive index sensitivity of 559.5 nm/RIU[16], yet its quality factor was merely 1 085. Therefore, for SOI-based refractive index sensors, achieving both high quality factors and sensitivity remains a significant research challenge.

We proposed a feedback waveguide slot grating micro-

ring resonator (FWSGMRR) structure. It was based on the U-shaped feedback waveguide slot micro-ring resonator with embedded air holes to form a grating structure. The grating reflected a part of the light, and the reflected light and micro-ring resonant light propagated in opposite directions, affecting each other and ultimately producing the EIT-like effect. Adjusting the physical parameters of the device achieved the EIT-like effect. The high slope characteristic of the EIT-like effect achieved a higher quality factor[17,18], resulting in a more obvious resonance wavelength shift and achieving higher sensitivity.

1 Basic principle

1.1 Structure design

The three-dimensional and planar views of the proposed structure are shown in Fig. 1(a) and 1(b). Fig.1(c) shows a magnified view of the coupling region. The structure is fabricated on an SOI platform, featuring a 2 μm thick SiO_2 substrate. The waveguide core layer is composed of Si with a thickness of 220 nm.

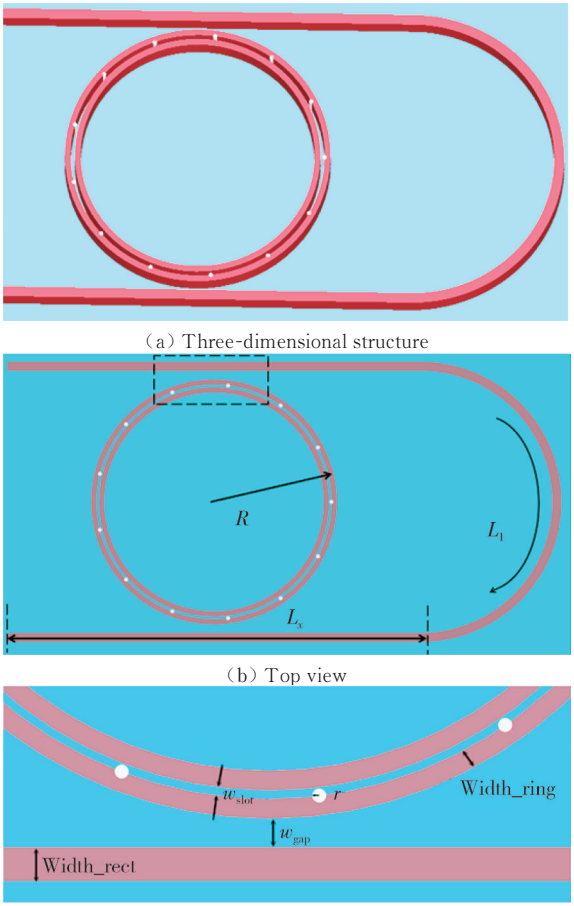

(a) Three-dimensional structure

(b) Top view

(c) Enlarged view of coupling zone

Fig. 1 FWSGMRR structure

The refractive indices are 1.444 for SiO_2 and 3.475 7 for Si. Fig.1(b) and 1(c) show the physical parameters of the structure. The width of the straight waveguide Width_rect is 0.42 μm. The width of the ring waveguide Width_ring is 0.24 μm. The straight waveguide length L_x is 17.2 μm. The coupling spacing w_{gap} is 0.33 μm. The length of the U-shaped feedback waveguide is L_1. The micro-ring has a radius of R, and the structure includes n embedded air holes, each with a radius of r, and the width of the slot is w_{slot}. We analyzed the effect of the above-mentioned parameters on the sensing performance of the proposed structure and optimized the structural parameters.

1.2 Theoretical analysis

The theoretical model of the structure is shown in Fig.2. The analysis of the transmission characteristics of the structure used the transmission matrix method. The t, k represent the transmission coefficient and coupling coefficient between the micro-ring and the straight waveguide. The transmission coefficients and coupling coefficients of the symmetrically coupled regions A and B are equal, and they satisfy $t^2 + k^2 = 1$ when the loss is zero.

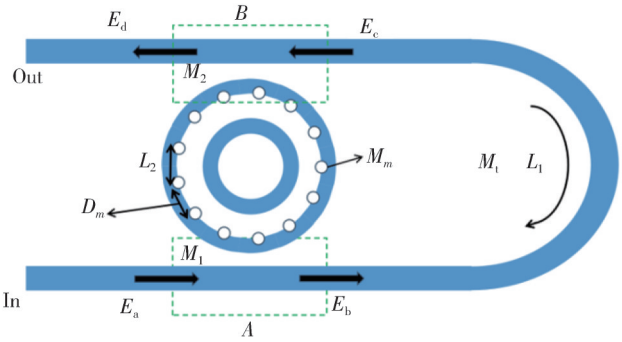

Fig. 2 Theoretical modeling of structure

$\boldsymbol{M}_1$, $\boldsymbol{M}_2$ are the transmission matrices between the microloop and the straight waveguide in the two coupling regions A and B, and $\boldsymbol{M}_t$ is the transmission matrix between the feedback waveguide and the microloop, then there are

$$\boldsymbol{M}_1 = \boldsymbol{M}_2 = \begin{bmatrix} \dfrac{-t}{ik} & \dfrac{1}{ik} \\ \dfrac{-1}{ik} & \dfrac{t}{ik} \end{bmatrix}, \tag{1}$$

$$\boldsymbol{M}_t = \begin{bmatrix} 0 & \tau^{\frac{1}{2}} p \\ (\tau^{\frac{1}{2}} p)^{-1} & 0 \end{bmatrix}, \tag{2}$$

where $\tau = \exp(-\alpha L)$ is the transmission coefficient of the optical signal inside the micro-ring. $L = 2\pi R$ is the circumference of the micro-ring, and α is the transmission loss coefficient. Here, $p = \exp(i\varphi/2)$ is

the phase factor of the optical signal when it is transmitted in the micro-ring for half of the circumference. $\varphi = \beta L$ is the phase difference of the light transmitted along the micro-ring for a complete loop, and $\beta = 2\pi n_{\text{eff}}/\lambda$ is the propagation constant.

Let the number of embedded air holes be n and the reflection coefficient of air holes be r_m, then the transmission matrix of the mth air holes is

$$\boldsymbol{M}_m = \frac{1}{\mathrm{i}\sqrt{1-r_m^2}}\begin{bmatrix} -1 & -r_m \\ r_m & 1 \end{bmatrix}, \tag{3}$$

where $m = 1, 2, 3, \cdots, n$.

It is also necessary to consider the effect produced by the attenuation of the grating cavities. The perimeter of the micro-ring is L. The number of air holes is n. And $L_2 = L/n$ is the length of the grating cavities, then the transmission matrix of the mth grating cavity[19] is

$$\boldsymbol{D}_m = \begin{bmatrix} \exp(\mathrm{i}2\pi n_{\text{eff}} L_2/\lambda) & 0 \\ 0 & \exp(-\mathrm{i}2\pi n_{\text{eff}} L_2/\lambda) \end{bmatrix}. \tag{4}$$

Then the total transmission matrix of the structure is

$$\boldsymbol{M} = \boldsymbol{M}_1 \boldsymbol{M}_t \boldsymbol{M}_2 \left(\prod_{m=1}^{n} \boldsymbol{M}_m \boldsymbol{D}_m \right) = \begin{bmatrix} M_{11} & M_{12} \\ M_{21} & M_{22} \end{bmatrix}. \tag{5}$$

Thus there is

$$\begin{bmatrix} E_{\text{d}} \\ E_{\text{c}} \end{bmatrix} = \boldsymbol{M} \begin{bmatrix} E_{\text{b}} \\ E_{\text{a}} \end{bmatrix}, \tag{6}$$

where $E_{\text{a}}, E_{\text{b}}, E_{\text{c}}, E_{\text{d}}$ are the light intensities of the ports.

And the relationship between the light field E_{c} and E_{b} is

$$E_{\text{c}} = \tau_1 p_1 E_{\text{b}}, \tag{7}$$

where $\tau_1 = \exp(-\alpha L_1)$ is the transmission coefficient of the optical signals in the feedback waveguide of length L_1, and $p_1 = \exp(\mathrm{i}\varphi_1)$ is the phase factor of the optical signals when they are transmitted within the feedback waveguide. $\varphi_1 = \beta L_1$ is the phase difference generated by the transmission of the optical signals from one end of the U-shaped feedback waveguide to the other end. From Eqs. (6) and (7), we can get

$$E_{\text{d}} = \left(M_{21} - \frac{M_{11} M_{22}}{M_{12} - \tau_1 p_1} \right) E_{\text{a}}. \tag{8}$$

When the structure has no feedback waveguide, the amplitude of the light field at the output is

$$E_o = \left(M_{21} - \frac{M_{11} M_{22}}{M_{12}} \right) E_{\text{a}}. \tag{9}$$

Thus Eq. (8) can also be expressed as

$$E_{\text{d}} = E_o + \frac{-\tau_1 p_1 M_{11} M_{22}}{M_{12}(M_{12} - \tau_1 p_1)} E_{\text{a}} = E_o + E_{\text{f}}, \tag{10}$$

where E_{f} is the additional optical field of the feedback waveguide.

The spectral expression at the output is

$$D = \left| \frac{E_{\text{d}}}{E_{\text{a}}} \right|^2 = \frac{|E_o|^2 + |E_{\text{f}}|^2 + 2|E_o||E_{\text{f}}|\cos\delta}{|E_{\text{a}}|^2}, \tag{11}$$

where δ is the phase difference between E_{o} and E_{f}.

2 Device structure optimization

The three-dimensional finite-difference time-domain method (3D-FDTD) was used to simulate the mode-field distribution of the structure as well as the transmission spectrum under different physical parameters. Four parameters, such as R, n, r, and w_{slot}, were optimized to improve the sensing performance of the device.

Fig. 3 illustrates the mode field distributions for both a single waveguide and a slot waveguide of the same dimensions. As shown in Fig. 3(a), the optical field in the slot structure is primarily concentrated within the slot, which has a lower refractive index, resulting in reduced optical dissipation. Consequently, the slot's ability to confine the optical field extends the interaction range between the optical field and the material being measured, thereby enhancing the sensing sensitivity.

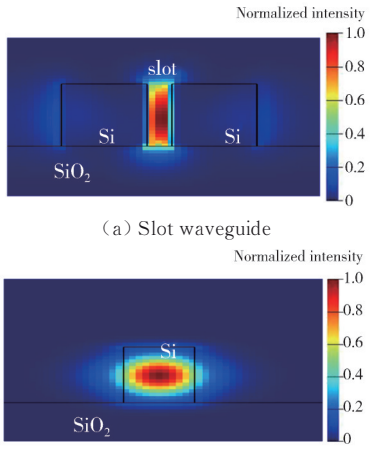

(a) Slot waveguide

(b) Strip waveguide

Fig. 3 Mode field distribution of two waveguides with same dimensions

The radius of the micro-ring waveguide significantly influences the bending loss and transmission loss of the resonator, necessitating its optimization to enhance the device's sensing performance. Fig. 4 depicts the variation in the quality factor as the radius R ranges from 4.5 to 5.2 μm. As observed in Fig. 4, the quality factor initially increases with R, reaching a peak at 5 μm, before declining. This trend occurs because, as R increases, the expansion of the effective coupling region allows more light to couple into the micro-ring and reduces bending loss, collectively

enhancing the quality factor. However, when R exceeds 5 μm, the quality factor diminishes. This decline is primarily due to the longer transmission path of the resonant light within the micro-ring, which increases transmission loss and consequently reduces the quality factor[20].

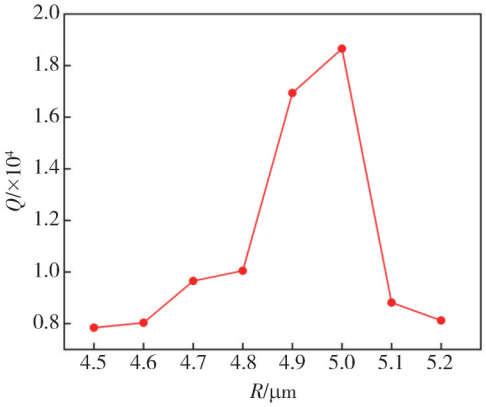

Fig. 4 Quality factor at different *R*

The centers of the air holes are positioned on the inner side of the outer micro-ring and arranged in a periodic pattern. The number of holes affects the effective refractive index of the reflecting surface, leading to varying splitting effects and influencing the Q factor. Fig. 5 analyzes the impact of n on both the Q factor and the number (N) of EIT-like peaks. As observed in the Fig. 5, the Q factor decreases as n increases. The heightened scattering loss caused by the air hole grating reduces the Q factor, which leads to this decline.

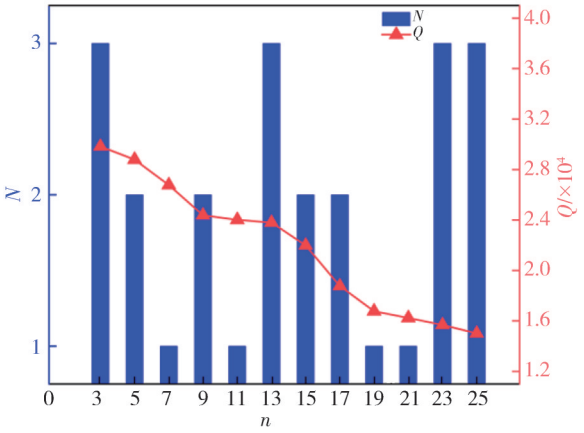

Fig. 5 Effect of *n* on *Q* and *N*

Fig. 6 presents the transmission spectrum of the device within the wavelength range of 1 500 to 1 600 nm for n =3, 13, 23, 25. It is evident that the device successfully achieves the splitting of three EIT-like peaks. Concurrently, as the number of air holes increases, the scattering loss also rises, leading to a reduction in the device's transmittance. When n is 3 and 13, the transmittance of the three resonance peaks remains above 0.9. The EIT-like spectral line is most pronounced when n is 13.

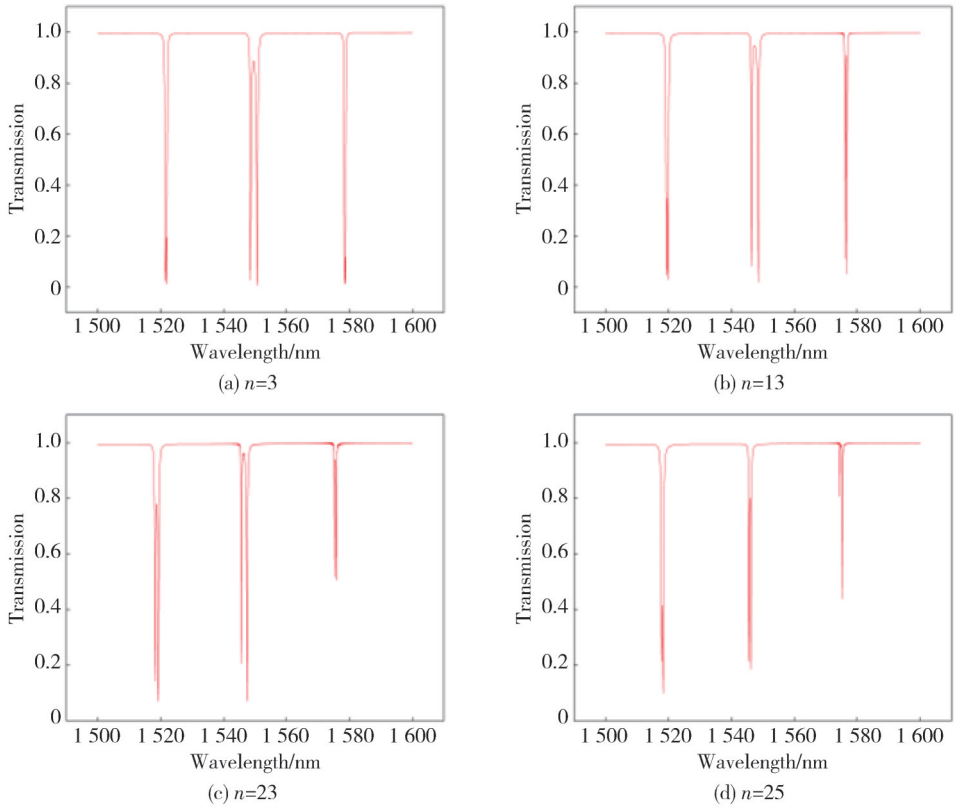

Fig. 6 Output spectrum with different number of *n*

Although the Q factor at that point is not optimal, it could be enhanced by later adjusting the w_{slot} and r parameters. Therefore, n is selected as 13, and the number of EIT-like peaks reaches the maximum value of

3, with the transmittance being above 0.9.

The unsmoothing and strong electric field interaction on the inner wall of the slot waveguide cause the slot waveguide to have greater loss than the ordinary waveguide. The lithography and etching process determine the size of the loss. The radius of the air holes located on the inner wall of the slot contributes to varying degrees of loss, thereby impacting both the Q factor and the extinction ratio (ER). The appropriate air holes radius should be selected when setting the air holes, otherwise the liquid to be tested will be difficult to enter the air holes, which will lead to the detection error. Under the premise that the liquid is sufficient to enter the air holes, the influence of r on the transmission spectrum, Q, and ER is shown in Fig.7.

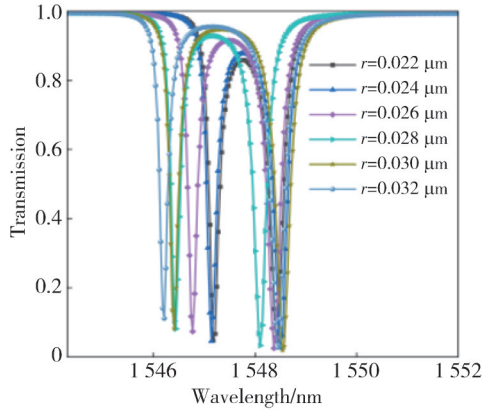

(a) Spectral line variation

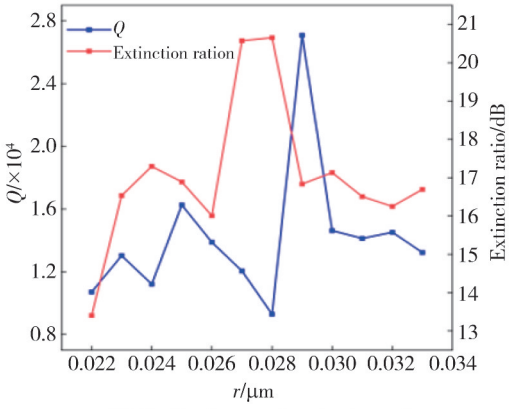

(b) Quality factor and extinction ratio

Fig. 7 Spectral changes of Q and ER at different r

Fig. 7(a) illustrates the changes in the transmission spectrum of the device for different values of r. As r increases, the peak of the transparent window in the EIT-like line shifts upward, while the resonance window moves to the left. Fig.7(b) shows the variation of the Q factor and ER with respect to r. When r is 0.029 μm, the Q factor reaches its maximum value of 27 088, and the ER is 16.836 8 dB. However, when r exceeds 0.029 μm, the Q factor decreases sharply. From a fabrication standpoint, creating this slot Bragg grating structure is more complex. Nevertheless, previous research successfully designed and fabricated a compact sensor based on an inner wall grating with a double groove, achieving an inner wall grating with a depth of 0.024 μm using photolithography[21]. Therefore, according to the current manufacturing process, the size of 0.029 μm mentioned in this paper can be achieved.

In optical refractive index sensors, the slot structure is typically exposed to the external environment, and the substance to be measured is completely covered and filled in the slot. Therefore, the slot width affects the action area of the light field and the substance to be measured[22,23]. If the slot width is too narrow, the substance to be measured is difficult to enter, which affects the sensing measurement. Conversely, if the width is too wide, the device's ability to confine the light field is diminished, leading to a reduced quality factor.

Fig.8 illustrates the variation of the quality factor and sensitivity (S) with respect to the slot width w_{slot}. Both Q and S initially increase with w_{slot} and then decrease. This behavior occurs because, as the w_{slot} increases, more energy is concentrated within the slot, leading to an increase in Q.

However, when the slot width reaches a certain point, some of the energy is scattered at the interface between the waveguide and the cladding, causing a decline in Q. When the w_{slot} is 0.051 μm, the Q and S achieve the maximum value at the same time, with Q being 59 267.5 and the sensitivity being 408.57 nm/RIU.

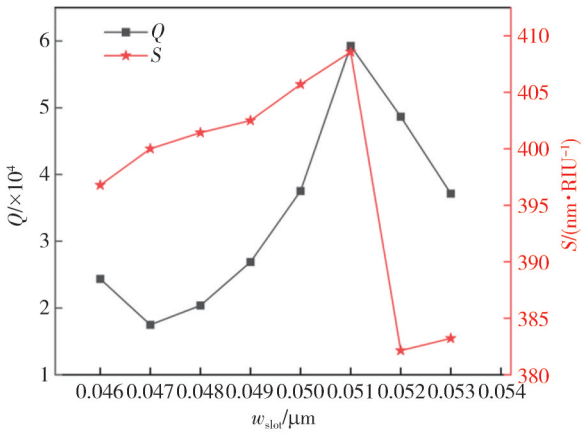

Fig. 8 Effect of w_{slot} on Q and S

At present, the nanoscale fabrication process of silicon-based materials still has much room for improvement. However, during the fabrication of devices with complex structures and nanoscale dimensions, certain errors may occur, causing the final results to deviate from expectations. To ensure the feasibility of the structure, we conducted a tolerance

analysis of r and w_{slot} based on the optimal conditions for all parameters. The influence of the fabrication error of r and w_{slot} on the device Q is analyzed with the fabrication error of $\pm$ 10 nm, as shown in Fig.9. It can be found that the minimum Q corresponding to r in the error range is 25 417.6, and the Q change is gentle in the range of 3 to 10 nm, showing good stability. The results presented in Fig. 9 demonstrate that the proposed structure exhibits excellent process tolerance.

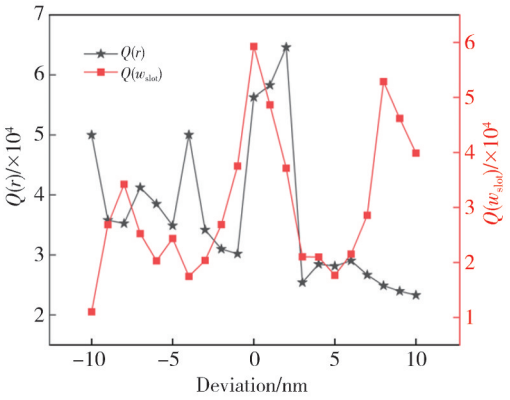

Fig. 9 Variation of Q within $\pm$ 10 nm of deviation for w_{slot} and r

3 Refractive index sensing characteristics

Sensing sensitivity (S) and limit of detection (LOD) are important indicators for evaluating the performance of the sensor, and their expressions are

$$S = \Delta\lambda_{res}/\Delta n, \tag{12}$$

$$LOD = \lambda/QS, \tag{13}$$

where $\Delta\lambda_{res}$ is the shift in resonant wavelength and Δn is the change in refractive index.

Under optimal conditions for all parameters, the sensor was placed in an environment where the refractive index was varied for sensing characterization. The ambient refractive index ranged from 1.333 2 to 1.339 2. This variation in the ambient refractive index results in a change in the device's effective refractive index, causing the resonance wavelength to shift. This shift is used to measure the refractive index sensitivity. Fig. 10 illustrates the transmission spectra and the changes in resonance wavelength at different refractive indices.

Fig. 10(a) shows the transmission spectra of the device at different ambient refractive indices. It can be found that the resonance wavelength is red-shifted to the right as the refractive index increases. Fig.10(b) shows the resonance wavelength of the device at different refractive indices. It can be found that the resonance wavelength and the refractive index have a good linear relationship with a sensitivity of 408.57 nm/RIU, while the fitting rate is more than 99%.

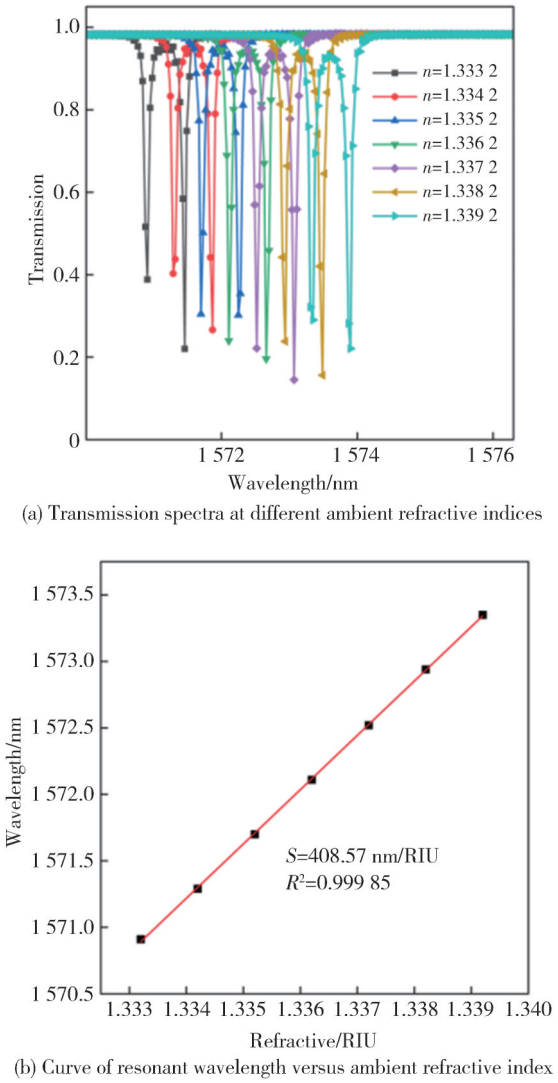

Fig. 10 Refractive index sensing analysis

Table 1 shows the comparison between the FWSGMRR structure and the MRR-based refractive index sensors proposed in the related literatures with respect to several parameters of Q, S, and LOD.

Table 1 Comparison of performance of proposed structure with MRR based refractive index sensor

Refractive index sensor	Q	S/(nm•RIU^{-1})	LOD/RIU
Ref.[13]	516	538	—
Ref.[14]	2 000	297.13	1.1×10^{-4}
Ref.[15]	190 000	86.371 4	—
Ref.[16]	1 085	559.5	2.2×10^{-5}
Ref.[23]	30 950	344	1.4×10^{-4}
Proposed structure	59 267.5	408.57	6.23×10^{-5}

By comparing with other refractive index sensors, it can be seen that the proposed structure has high quality factor and sensitivity at the same time. In the sensing application the sensitivity of this structure reaches 408.57 nm/RIU, with a detection limit of 6.23×10^{-5} RIU, and Q of 59 267.5 at the same time.

This type of micro-ring resonator is versatile, finding applications not only in refractive index sensing[24] but also in temperature sensing and the medical field for detecting changes in environmental temperature or hemoglobin concentration. For example, in the industrial field, factories will produce CO_2 emissions, and some factories will produce clean energy such as H_2 that is easy to explode. In such scenarios, sensor detection becomes crucial for ensuring production safety and preventing environmental pollution. A polymer micro-ring resonator array was fabricated to simultaneously detect CO_2 and H_2, helping to assess whether a plant's gas emissions meet regulatory standards[25]. And it was small in size and easy to integrate. Micro-ring sensors can be used not only for the detection of inorganic substances, but also for the detection of volatile organic compounds such as acetone[26]. Micro-ring sensors is also used in the biomedical field to detect antigens and antibodies[27], such as using the reaction of anti-DNA and miRNAs to detect miRNAs[28], or to detect hemoglobin[29] in the blood or nucleocapsid protein of SARS-CoV-2[30]. In addition, micro-ring sensors are also used in agronomy, such as the detection of beanpod mottle virus[31] to prevent soybean pests and diseases, thereby increasing soybean yield. It can be seen that the micro-ring sensor is widely used and has good development prospects[32].

4 Conclusions

A feedback waveguide slot grating micro-ring resonator was designed to realize the coupling structure between the slot micro-ring and Bragg grating by embedding air holes in the slot. Two different optical modes of the slot micro-ring and Bragg grating interfered in different optical paths, resulting in the EIT-like effect. The parameters such as R, n, r, and w_{slot} were simulated and optimized using Lumerical software, and a tolerance analysis of the structural parameters was performed. The results showed that the proposed structure was reliable and realizable. In refractive index sensing, the sensitivity reaches 408.57 nm/RIU, with a detection limit of 6.23×10^{-5} RIU, and a quality factor of 59 267.5. It showed that the proposed structure had good performance and was easy to integrate, suitable for application in sensing arrays, and had a great potential in the field of optical sensing.

Acknowledgement

This work was supported by Natural Science Foundation of Gansu Province (NO. 21JR7RA289)

Declaration of conflicting interests

The authors have no conflict of interests related to this publication.

References

[1] SUN L, ZHANG Y, HE Y, et al. Subwavelength structured silicon waveguides and photonic devices. Nanophotonics, 2020, 9(6): 1321-1340.

[2] ZHANG X, ZHOU G, SHI P, et al. On-chip integrated optofluidic complex refractive index sensing using silicon photonic crystal nanobeam cavities. Optics Letters, 2016, 41(6): 1197-1200.

[3] XING E B, LI J L, RONG J M, et al. Fabrication of ultrahigh optical quality factor crystalline resonator and prism coupling package. Journal of Test and Measurement Technology, 2022, 36(4): 277-280.

[4] AMIRI I S, ARIANNEJAD M M, DAUD S, et al. High sensitive temperature sensor silicon-based microring resonator using the broadband input spectrum. Results in Physics, 2018, 9: 1578-1584.

[5] WANG Z, WANG D, DENG F, et al. Ag quantum dots decorated ultrathin g-C_3N_4 nanosheets for boosting degradation of pharmaceutical contaminants: insight from interfacial electric field induced by local surface plasma resonance. Chemical Engineering Journal, 2023, 463: 142313.

[6] PUUMALA L S, GRIST S M, WICKREMASINGHE K, et al. An optimization framework for silicon photonic evanescent-field biosensors using sub-wavelength gratings. Biosensors, 2022, 12(10): 840.

[7] KISKU S, SARWAGYA K, RANJAN S. Performance investigation of triple unsymmetrical micro ring resonator as optical filter as well as biosensor. Optical and Quantum Electronics, 2023, 55(2): 164.

[8] SINGH A K, MITTAL S, DAS M, et al. Optical biosensors: a decade in review. Alexandria Engineering Journal, 2023, 67: 673-691.

[9] WANG S, LIU Y, ZHAO D, et al. Optofluidic Fano resonance photonic crystal refractometric sensors. Applied Physics Letters, 2017, 110(9): 091105.

[10] LU Y, FU X, CHU D, et al. Fano resonance and spectral compression in a ring resonator drop filter with feedback. Optics Communications, 2011, 284(1): 476-479.

[11] MIAO M K, XIAO J J, XIA D, et al. Tunable Fano-like resonance with ultra-high slope rate via nonlinear interference in a chalcogenide microring resonator. Journal of Lightwave Technology, 2025, 43(2): 665-673.

[12] GU L, FANG L, FANG H, et al. Fano resonance lineshapes in a waveguide-microring structure enabled by an air-hole. APL Photonics, 2020, 5(1): 016108.

[13] GABALIS M, URBONAS D, PETRUSKEVICIUS R. A perforated microring resonator for optical sensing

applications. Journal of Optics, 2014, 16(10): 105003.
[14] ZHAO C Y, ZHANG L, ZHANG C M. Compact SOI optimized slot microring coupled phase-shifted Bragg grating resonator for sensing. Optics Communications, 2018, 414: 212-216.
[15] WU N S, LI X. High-Q optical filter based on multi-nanohole micro-ring resonator//2018 Asia Communications and Photonics Conference, October 26-29, 2018, Hangzhou, China. New York: IEEE, 2018: 1-2.
[16] GU H, GONG H, WANG C, et al. Compact inner-wall grating slot microring resonator for label-free sensing. Sensors, 2019, 19(22): 5038.
[17] ZHANG Z, NG G I, HU T, et al. Electromagnetically induced transparency-like effect in microring-bragg gratings based coupling resonant system. Optics Express, 2016, 24(22): 25665-25675.
[18] LIU C, SANG C, WU X, et al. Grating double-slot micro-ring resonator for sensing. Optics Communications, 2021, 499: 127280.
[19] GU L, FANG H, LI J, et al. A compact structure for realizing Lorentzian, Fano, and electromagnetically induced transparency resonance lineshapes in a microring resonator. Nanophotonics, 2019, 8(5): 841-848.
[20] SONG J H, KONGNYUY T D, HEYN P D, et al. Low-loss waveguide bends by advanced shape for photonic integrated circuits. Journal of Lightwave Technology, 2020, 38(12): 3273-3279.
[21] CHENG W Q, YE S W, SUN X, et al. Double slot micro ring resonators with inner wall angular gratings as ultra highly sensitive biochemical sensors//2022 IEEE Photonics Conference, November 13-17, 2022, Vancouver, Canada. New York: IEEE, 2022: 1-2.
[22] OZCAN C, AITCHISON J S, MOJAHEDI M. Optimization of bulk sensitivity for strip, slot, and subwavelength grating-based waveguides for dual-polarization operation. Optics Express, 2023, 31(3): 3579-3594.
[23] LIU C, SANG C, WU X, et al. One-dimensional photonic crystal groove microring resonators and its sensing characteristics. Acta Optica Sinica, 2020, 40(24): 2413002.
[24] CAO Q Q, LIU C J, WU X S, et al. Asymmetrical Fabry-Perot cavity slot micro-ring resonator and its sensing characteristics. Journal of Measurement Science and Instrumentation, 2024, 15(3): 292-301.
[25] MI G, HORVATH C, VAN V. Silicon photonic dual-gas sensor for H_2 and CO_2 detection. Optics Express, 2017, 25: 16250.
[26] ZHANG G J, FENG X L, LIEBDERG B, et al. Gas sensor for volatile organic compounds detection using silicon photonic ring resonator. Procedia Engineering, 2016, 168: 1771-1774.
[27] TANIGUCHI T, HIROWATARI A, IKEDA T, et al. Detection of antibody-antigen reaction by silicon nitride slot-ring biosensors using protein G. Optics Communications, 2016, 365: 16-23.
[28] QAVI A J, KINDT J T, GLEESON M A G, et al. Anti-DNA: RNA antibodies and silicon photonic microring resonators: increased sensitivity for multiplexed microRNA detection. Analytical Chemistry, 2011, 83(15): 5949-5956.
[29] AJAD A K, ISLAM M J, KAYSIR M R, et al. Highly sensitive bio sensor based on WGM ring resonator for hemoglobin detection in blood samples. Optik, 2021, 226: 166009.
[30] UCHIDA Y, ARAKAWA T, HIGO A, et al. Silicon microring resonator biosensor for detection of nucleocapsid protein of SARS-CoV-2. Sensors, 2024, 24(10): 3250.
[31] MCCLELLAN M S, DOMIRE L L, BAILEY R C. Label-free virus detection using silicon photonic microring resonators. Biosensors and Bioelectronics, 2012, 31(1): 388-392.
[32] STEGELICH P, HULSEMANN M, DIETZEL B, et al. Optical biosensors based on silicon-on-insulator ring resonators: a review. Molecules, 2019, 24(3): 519.

反馈波导狭缝光栅微环谐振器的传感特性

朱彦杰，梁龙学*，刘春娟

兰州交通大学 电子与信息工程学院，甘肃 兰州 730070

摘　要： 为提高折射率传感器的品质因数和灵敏度，本文提出了一种反馈波导狭缝光栅微环谐振器。该结构在狭缝微环的基础上引入气孔光栅结构，利用光栅的反射以实现不同波长处的类电磁诱导透明效应，类电磁诱导透明效应的高斜率特性可以实现更高的品质因数和灵敏度。采用传输矩阵法分析结构的传输原理，利用时域有限差分法对结构的传输频谱和模场分布进行模拟仿真，并调整器件结构参数进行优化。仿真结果表明：所提结构实现了类电磁诱导透明效应，品质因数为59 267.5。在折射率传感特性分析中，该结构的灵敏度为408.57 nm/RIU，同时，探测极限达到了6.23×10^{-5} RIU。所提结构同时实现了较高的品质因数和折射率灵敏度，在传感检测方面拥有良好的传感性能，在环境监测和生物医学等方面拥有广泛的应用市场。

关键词： 集成光学；微环谐振器；狭缝微环；光栅；折射率传感器；硅基波导

引用格式： ZHU Yanjie, LIANG Longxue, LIU Chunjuan. Sensing characteristics of feedback waveguide slot grating microring resonators. Journal of Measurement Science and Instrumentation, 2025, 16(2): 272-279. DOI: 10.62756/jmsi.1674-8042.2025026